Electronic Supplementary Material (ESI) for Energy Advances.

Supporting Information –

Pressure Dependence of Ionic Conductivity in Site Disordered Lithium Superionic Argyrodite Li_6PS_5Br

Vasiliki Faka,[a] Matthias T. Agne,[b] Paul Till,[a] Tim Bernges,[a] Marcel Sadowski,[c] Ajay Gautam,[a] Karsten Albe,[c] Wolfgang G. Zeier*[a,b]

[a] *Institute of Inorganic and Analytical Chemistry, University of Münster, Correnstraße 30, 48149 Münster, Germany.*

[b] *Institut für Energie- und Klimaforschung (IEK), IEK-12: Helmholtz-Institut Münster, Forschungszentrum Jülich, 48149 Münster, Germany.*

[c] *Department of Materials Science, Technical University of Darmstadt, Otto-Berndt-Strasse 3, D-64287 Darmstadt, Germany.*

E-mail:

*wzeier@uni-muenster.de

Derivation of activation volume

The activation volume as a thermodynamic quantity is defined as the variation of the change in Gibbs free energy with pressure as:

$$\left(\frac{\partial \Delta G}{\partial p}\right)_T = \Delta V_{\mathrm{a}} \tag{S1}$$

Ionic transport in solids occurs via a defect-mediated diffusion mechanism and the Gibbs free energy for the ionic jump (Δ*G*) is related to the formation volume ($V_{\mathrm{D}}^{\mathrm{F}}$) of defects (such as vacancies, interstitials, anti-site defects etc.) and to the migration volume ($V_{\mathrm{D}}^{\mathrm{M}}$) related to the motion of a cation (eq. 3):[1,2]

$$\left(\frac{\partial \Delta G_{\mathrm{f}}}{\partial p}\right)_T = V_{\mathrm{D}}^{\mathrm{F}} \tag{S2}$$

$$\left(\frac{\partial \Delta G_{\mathrm{m}}}{\partial p}\right)_T = V_{\mathrm{D}}^{\mathrm{M}} \tag{S3}$$

Therefore, the activation volume is equal to $\Delta V_{\mathrm{a}} = V_{\mathrm{D}}^{\mathrm{F}} + V_{\mathrm{D}}^{\mathrm{M}}$ (S4)

In the intrinsic region (i.e., at high temperatures), ΔG_{d} corresponds to the free energy of defect formation and is related to the temperature-dependent creation of cation and anion vacancies (namely Schottky pairs), requiring full consideration of Eq. S1. In the extrinsic region, however, the defect concentrations are largely temperature independent, i.e. $\Delta G \approx \Delta G_{\mathrm{m}}$, and the dominant contribution to the activation volume is from the migration of cation vacancies because anion vacancies are much less mobile.[3] Here, we assume that $\Delta G_{\mathrm{d}} \approx 0$ in fast ionic conductors near room temperature, therefore the activation volume is related only to the migration of the cations[2] and can be expressed by the pressure dependence of the ionic conductivity *σ*, as:

$$\sigma = \frac{\sigma_0}{T} \exp\left(-\frac{\Delta G}{k_B T}\right) \tag{S4}$$

The activation volume is defined as the variation of the change in Gibbs free energy Δ*G* with pressure *p*:

$$\Delta V_{\mathrm{a}} = \frac{\partial(\Delta G)}{\partial p}\Big|_T = \frac{\partial}{\partial p}\left(-k_B T[\ln(\sigma T) - \ln(\sigma_0)]\right)\Big|_T \tag{S5}$$

$$\Delta V_{\mathrm{a}} = \frac{\partial(\Delta G)}{\partial p}\Big|_T = -k_B T \frac{\partial \ln(\sigma T)}{\partial p} + k_B T \frac{\partial \ln(\sigma_0)}{\partial p} \tag{S6}$$

The first term in (S6) can be extracted from the pressure-dependent ionic conductivities measurements, while the second term in (S6) includes pressure-independent terms.

Assuming $\sigma_0 = C{\alpha_0}^2 \nu$, with a pressure-independent term *C* and pressure-dependent jump distance (α_0) and frequency (ν), then:

$$\Delta V_{\mathrm{a}} = k_B T \left[\frac{\partial \ln(\sigma_0)}{\partial p} - \frac{\partial \ln(\sigma T)}{\partial p}\right]|_T = k_B T \left[\frac{\partial \ln(\alpha_0{}^2)}{\partial p} + \frac{\partial \ln(\nu)}{\partial p} - \frac{\partial \ln(\sigma T)}{\partial p}\right]|_T \quad \text{(S7)}$$

The jump distance α_0 can vary like the lattice parameter α and can be written in terms of the unit cell volume V as

$$a = V^{1/3} \quad \text{(S8)}$$

Then

$$\frac{\partial \ln(a^2)}{\partial p} = \frac{2}{3}\frac{\partial \ln(V)}{\partial p} = -\frac{2}{3}\beta \quad \text{(S9)}$$

Where β is the lattice compressibility, equals to:

$$\beta = -\frac{\partial \ln(V)}{\partial p}|_T \quad \text{(S10)}$$

Using the chain rule expansion:

$$\frac{\partial \ln(\nu)}{\partial p}|_T = \frac{\partial \ln(\nu)}{\partial \ln(V)}|_T \frac{\partial \ln(V)}{\partial p}|_T = \gamma\beta \quad \text{(S11)}$$

With *γ* to be the microscopic Grüneisen parameter:

$$\gamma = -\frac{\partial \ln(\nu)}{\partial \ln(V)} \quad \text{(S12)}$$

Substituting

$$\Delta V_{\mathrm{a}} = k_B T \left[-\frac{2}{3}\beta + \gamma\beta - \frac{\partial \ln(\sigma T)}{\partial p}\right]|_T = k_B T \left[\beta\left(\gamma - \frac{2}{3}\right) - \frac{\partial \ln(\sigma T)}{\partial p}\right]|_T \quad \text{(S13)}$$

We have to mention here that the so-called migration volume of the microscopic picture (V_{m}) does not have the same meaning as the migration volume of the thermodynamic perspective ($V_{\mathrm{D}}^{\mathrm{M}}$), which refers to the motion of a cation. In the thermodynamic perspective, the migration volume is equal to the activation volume, when the formation volume of the defects is zero.

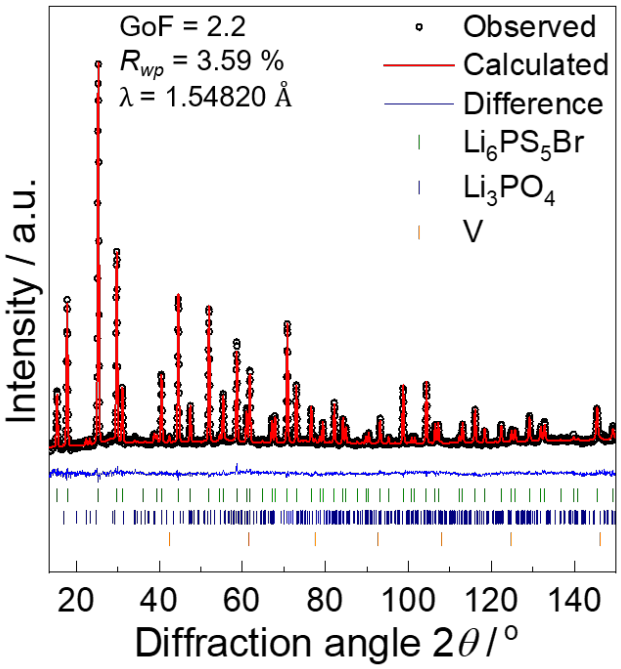

Figure S1: *Neutron diffraction data and the corresponding Rietveld refinement of the 10% Br^-/S^{2-} site-disordered Li_6PS_5Br. The black circles represent the experimental data and the red line shows the calculated pattern. The blue line denotes the difference profile. The green, blue and orange vertical lines denote the Bragg reflection position from Li_6PS_5Br, Li_3PO_4 and Vanadium sample holder, respectively.*

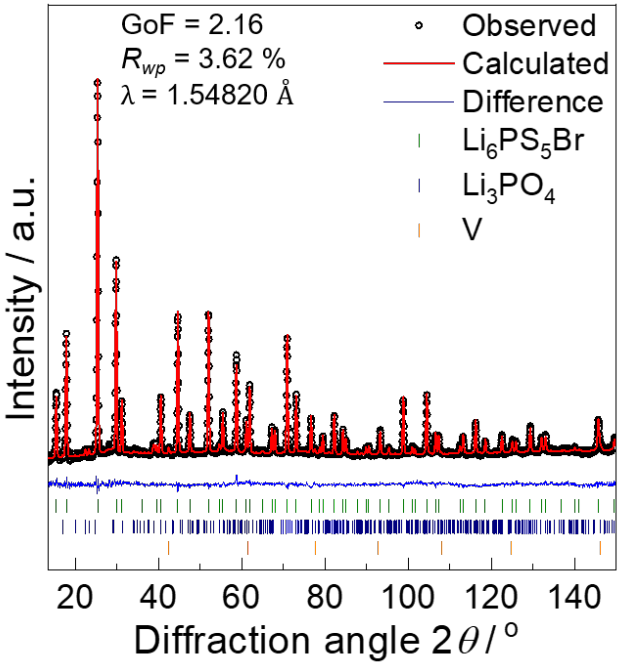

Figure S2: *Neutron diffraction data and the corresponding Rietveld refinement of the 18% Br^-/S^{2-} site-disordered Li_6PS_5Br. The black circles represent the experimental data and the red line shows the calculated pattern. The blue line denotes the difference profile. The green, blue and orange vertical lines denote the Bragg reflection position from Li_6PS_5Br, Li_3PO_4 and Vanadium sample holder, respectively.*

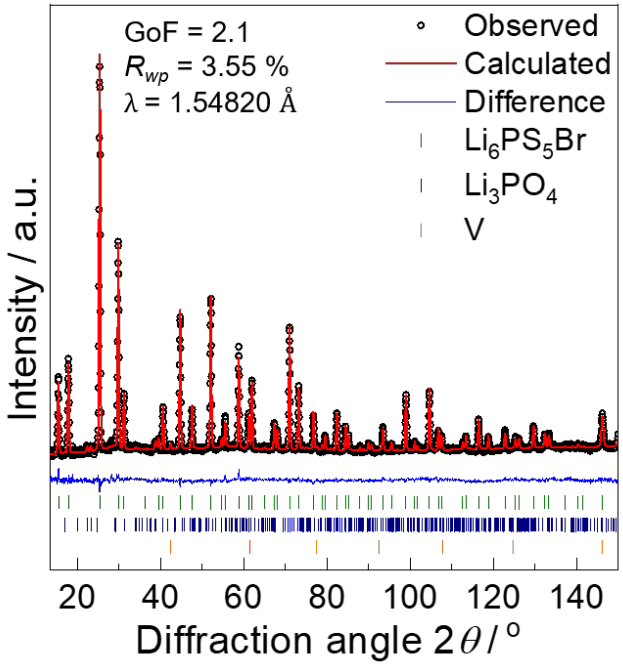

Figure S3. *Neutron diffraction data and the corresponding Rietveld refinement of the 28% Br^-/S^{2-} site-disordered Li_6PS_5Br. The black circles represent the experimental data and the red line shows the calculated pattern. The blue line denotes the difference profile. The green, blue and orange vertical lines denote the Bragg reflection position from Li_6PS_5Br, Li_3PO_4 and Vanadium sample holder, respectively.*

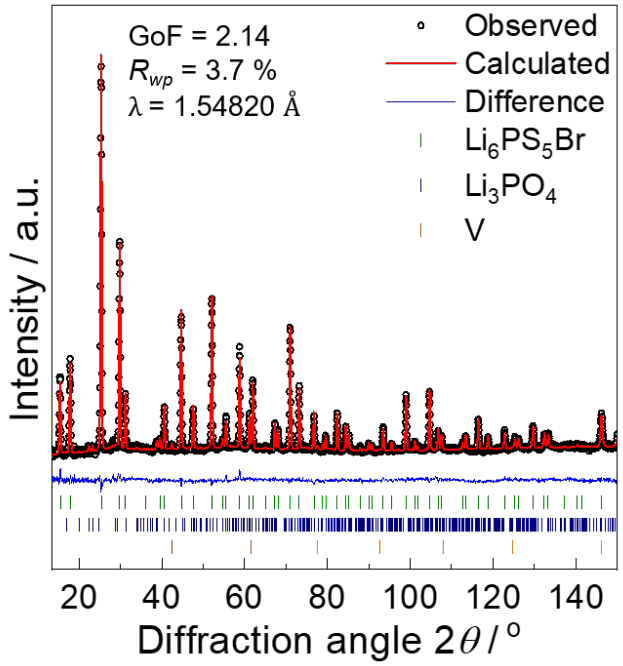

Figure S4: *Neutron diffraction data and the corresponding Rietveld refinement of the 34% Br^-/S^{2-} site-disordered Li_6PS_5Br. The black circles represent the experimental data and the red line shows the calculated pattern. The blue line denotes the difference profile. The green, blue and orange vertical lines denote the Bragg reflection position from Li_6PS_5Br, Li_3PO_4 and Vanadium sample holder, respectively.*

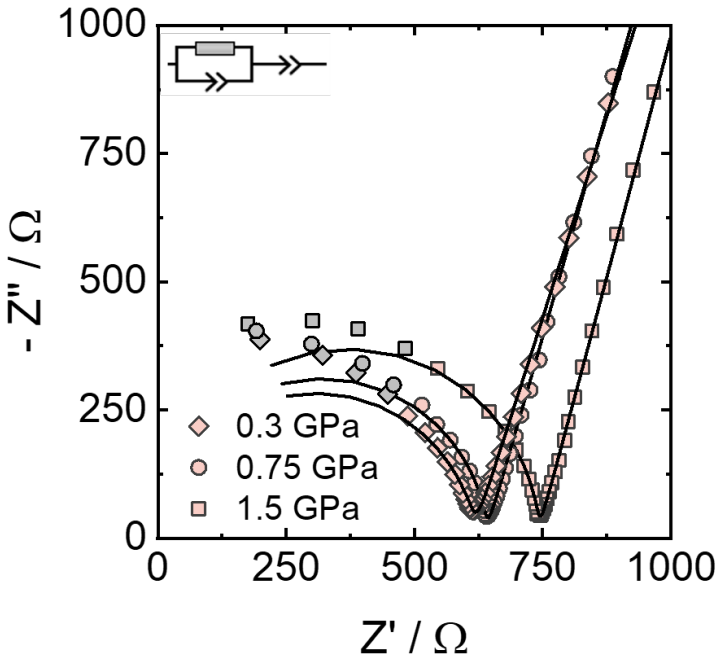

Figure S5: *Representative Nyquist plot impedance spectra of 10% Br^-/S^{2-} site-disordered Li_6PS_5Br under three different applied pressures (0.3 GPa, 0.75 GPa and 1.5 GPa) upon decompression. The black lines represent the obtained fit to the data, according to the depicted equivalent circuit. The grey-shaded data points represent the data that were not included into the fitting process, after evaluating the data with the Kramer-Kronig analysis. The impedance data were fit with an equivalent circuit consisting of a parallel resistor/constant phase element (CPE) in series with a CPE.*

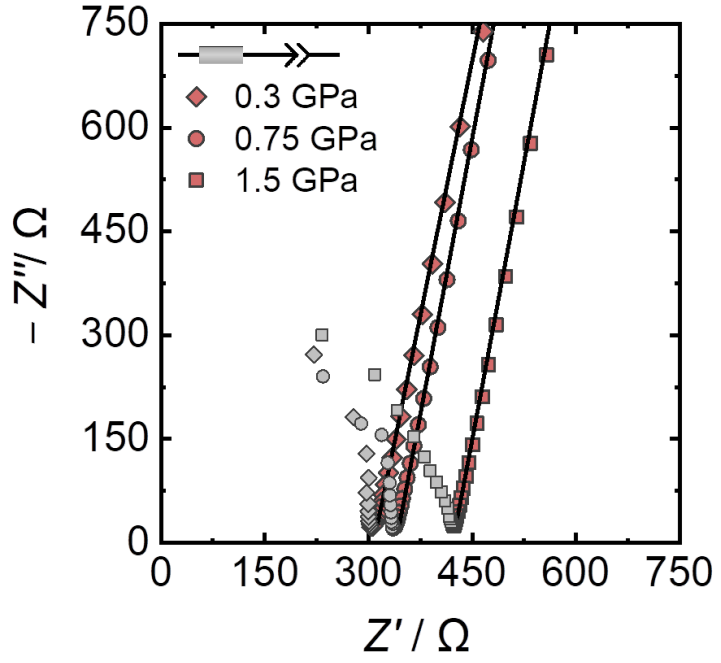

Figure S6: *Representative Nyquist plot impedance spectra of 18% Br^-/S^{2-} site-disordered Li_6PS_5Br under three different applied pressures (0.3 GPa, 0.75 GPa and 1.5 GPa) upon decompression. The black lines represent the obtained fit to the data, according to the depicted equivalent circuit. The grey-shaded data points represent the data that were not included into the fitting process, after evaluating the data with the Kramer-Kronig analysis. The impedance data were fit with an equivalent circuit consisting of a resistor in series with a constant phase element (CPE).*

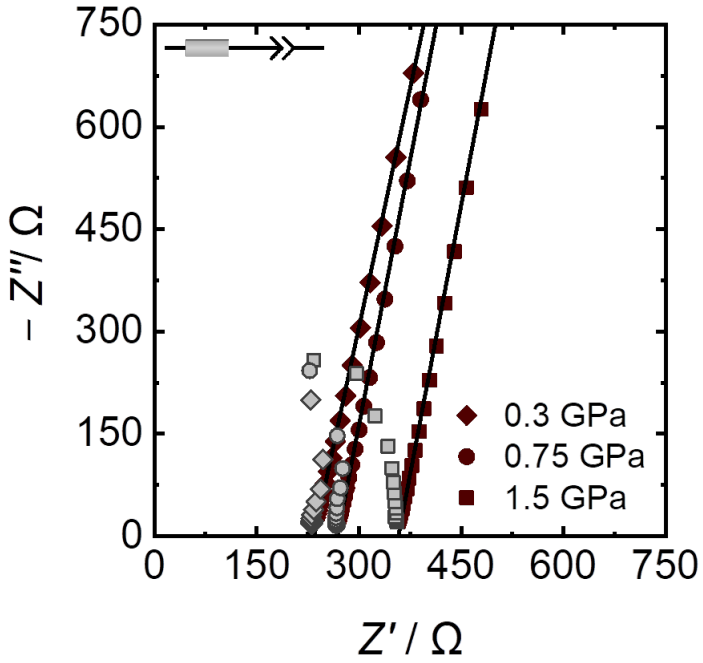

Figure S7: *Representative Nyquist plot impedance spectra of 34% Br^-/S^{2-} site-disordered Li_6PS_5Br under three different applied pressures (0.3 GPa, 0.75 GPa and 1.5 GPa) upon decompression. The black lines represent the obtained fit to the data, according to the depicted equivalent circuit. The grey-shaded data points represent the data that were not included into the fitting process, after evaluating the data with the Kramer-Kronig analysis. The impedance data were fit with an equivalent circuit consisting of a resistor in series with a constant phase element (CPE).*

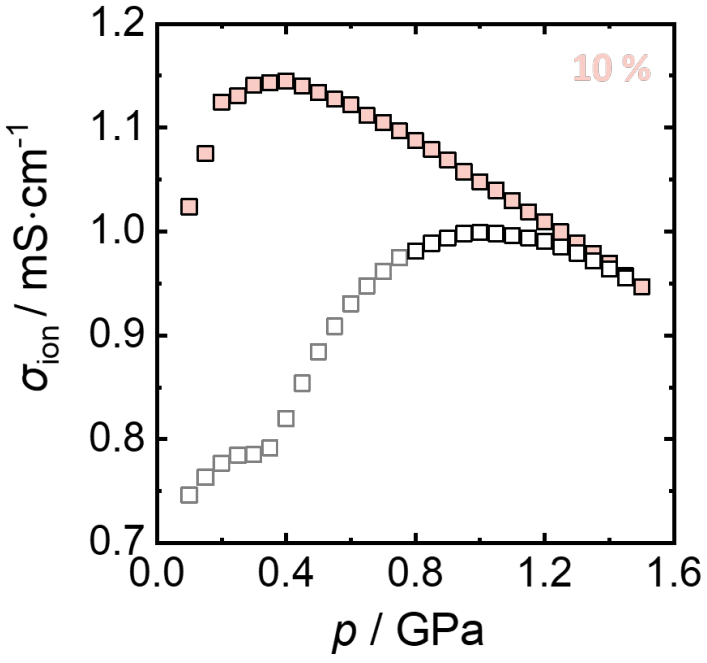

Figure S8: *Pressure-dependent ionic conductivity data of 10% Br^-/S^{2-} site-disordered Li_6PS_5Br in a range of 0.1 GPa to 1.5 GPa with a measurement step of 0.05 GPa. The material was pressed at 370 MPa before cycling in the full range of pressures. The open-shaped grey data points refer to the densification regime. The open-shaped black data points correspond to the compression of the material with the increasing pressures. The pink colored dots depicted the decompression from 1.5 GPa to 0.1 GPa.*

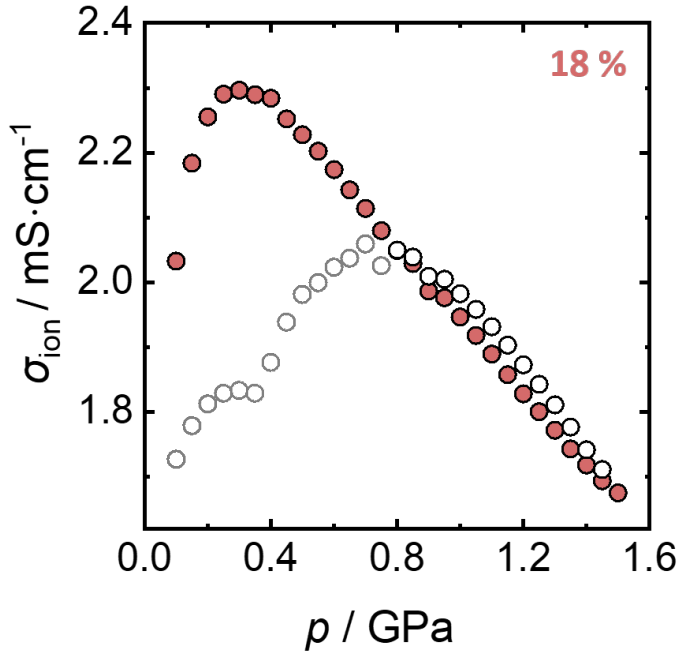

Figure S9: *Pressure-dependent ionic conductivity data of 18% Br^-/S^{2-} site-disordered Li_6PS_5Br in a range of 0.1 GPa to 1.5 GPa with a measurement step of 0.05 GPa. The material was pressed at 370 MPa before cycling in the full range of pressures. The open-shaped grey data points refer to the densification regime. The open-shaped black data points correspond to the compression of the material with the increasing pressures. The colored dots depicted the decompression from 1.5 GPa to 0.1 GPa.*

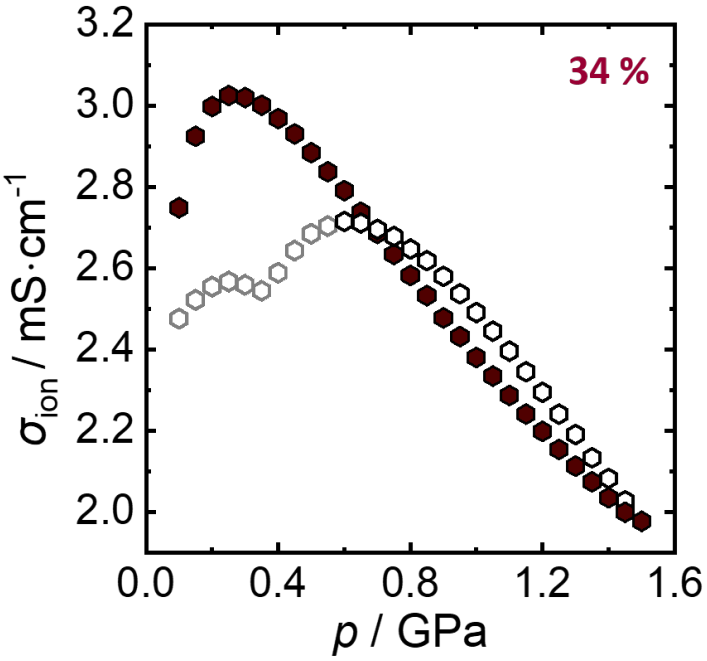

Figure S10: *Pressure-dependent ionic conductivity data of 34% Br^-/S^{2-} site-disordered Li_6PS_5Br in a range of 0.1 GPa to 1.5 GPa with a measurement step of 0.05 GPa. The material was pressed at 370 MPa before cycling in the full range of pressures. The open-shaped grey data points refer to the densification regime. The open-shaped black data points correspond to the compression of the material with the increasing pressures. The colored dots depicted the decompression from 1.5 GPa to 0.1 GPa.*

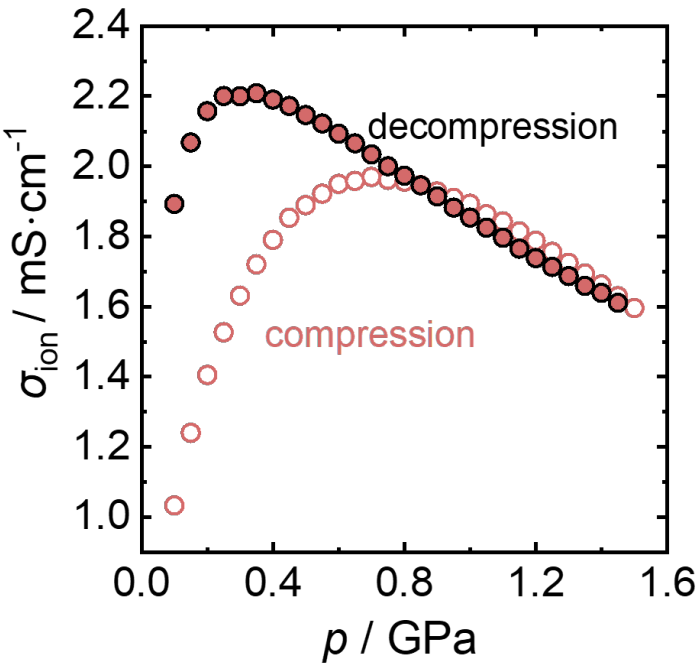

Figure S11: *The evolution of ionic conductivity upon applied pressure of 18% Br^{-}/S^{2-} site-disordered Li_6PS_5Br, without applying the initial pressure at 370 MPa on the material, where it can be seen the absence of the artifact at 370 MPa.*

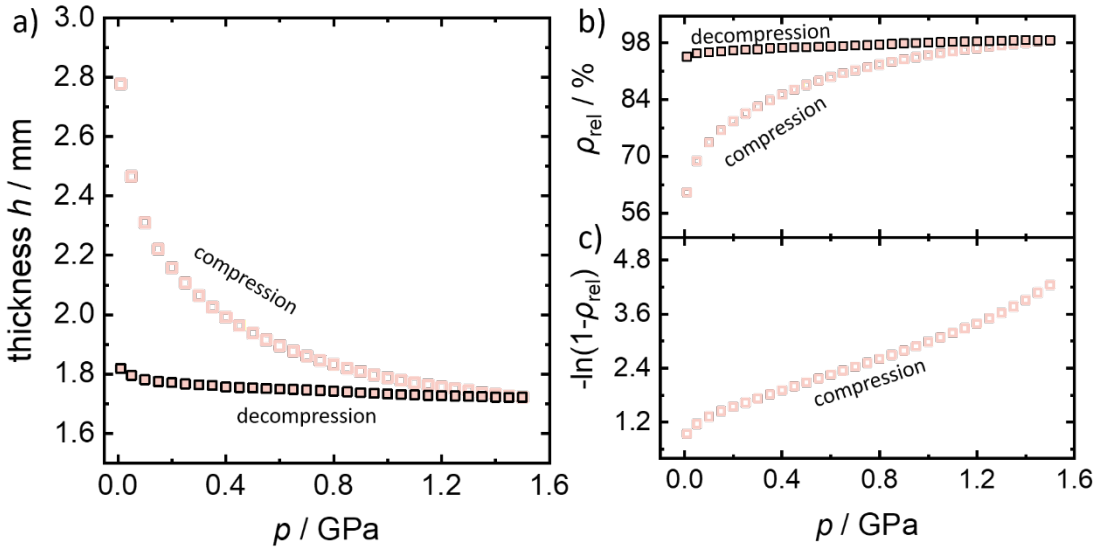

Figure S12: *(a) The consolidation of the powder and the simultaneous change in thickness can be calculated from the displacement of the pistons of the measurement setup. (b) The changes in relative density can be monitored for different pressures. The powder at 1.5 GPa has a relative density of 99%. (c) The Heckel plot upon compression can be calculated from the changes in the relative density and it shows the distinction of different coMPaction regimes when pressure is applied.*

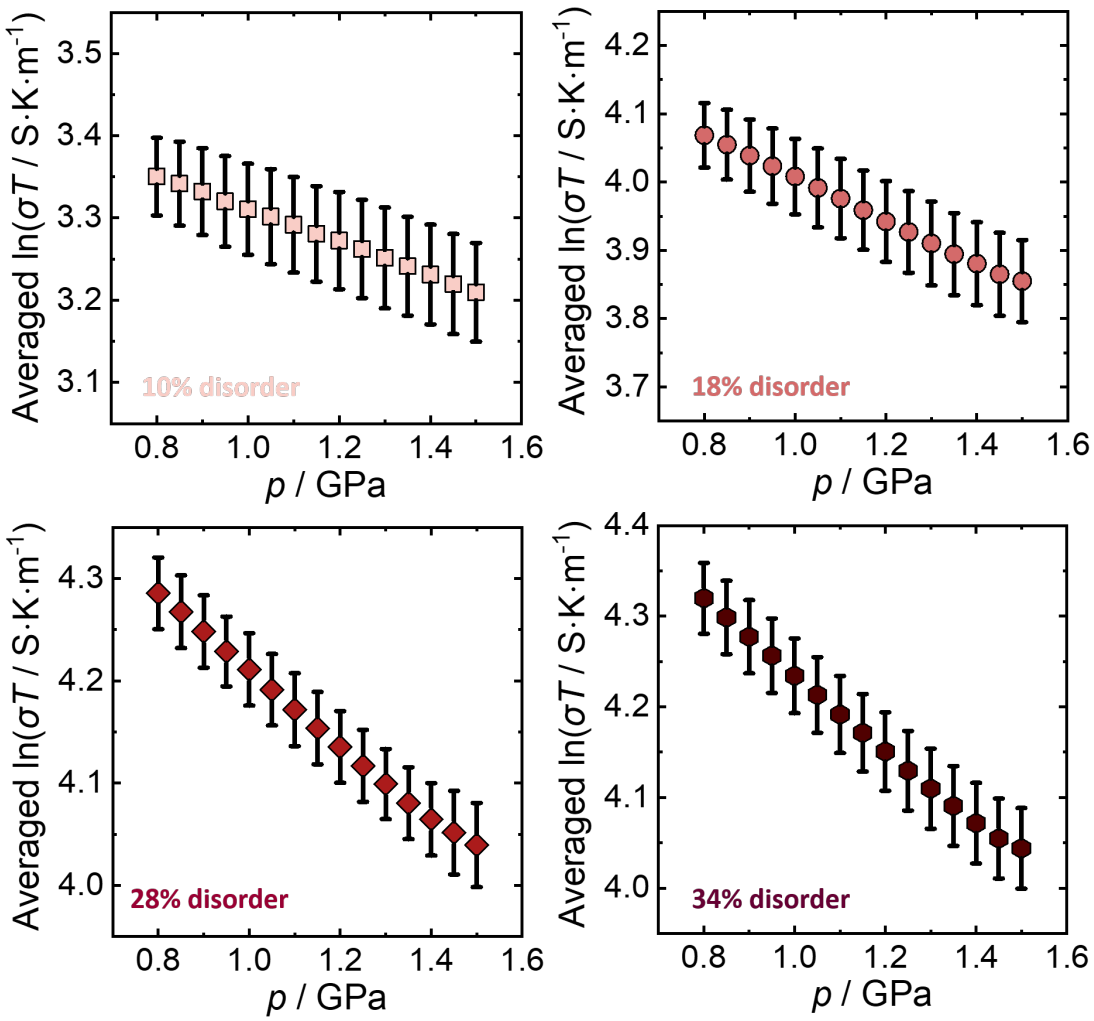

Figure S13: *The relationship between the logarithm of ionic conductivity and their uncertainties calculated from triplicate measurements vs. pressure for all the Br^{-}/S^{2-} site disordered lithium argyrodites.*

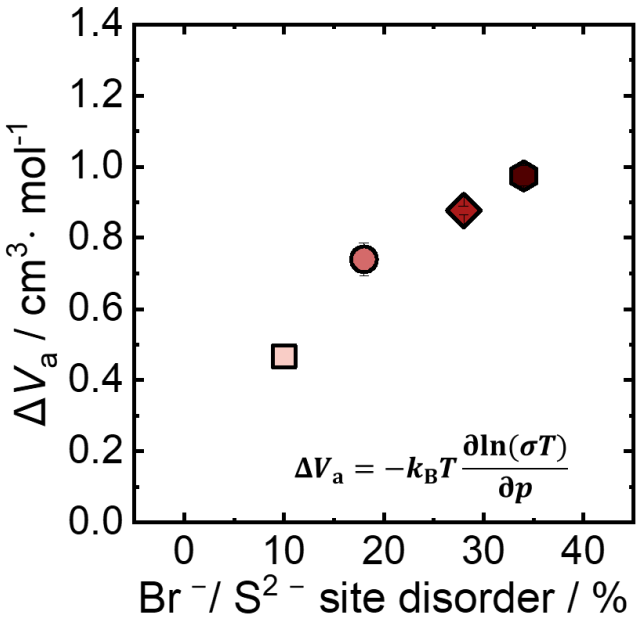

Figure S14: *Calculated activation volume values for all the different disorders using the simplified equation (without including β and γ), where the slope is the logarithm of the ionic conductivity versus applied pressure. The values are depicted in cm^3/mol in accordance to the literature.*

	Using Eq. 4 (Simplified Eq.)	Using Eq. 3 (Eq. including β and γ)
Br^-/S^{2-} site disorder / %	$\Delta V_a \pm 0.04$ cm^3/mol	$\Delta V_a \pm 0.04$ cm^3/mol
10	0.47	0.58
18	0.74	0.85
28	0.88	0.99
34	0.97	1.09

Table S1: *Calculated activation volume values in cm^3/mol for all the different disorders, by using the simplified equation (Eq. 4) and the extended Eq. 3, where compressibility β Gruneisen parameter γ are included.*

	Using Eq. 3 (Eq. including β and γ)	
Br^-/S^{2-} site disorder / %	ΔV_a cm^3/mol	ΔV_a Å^3/atom
10	0.58 ± 0.04	0.96 ± 0.04
18	0.85 ± 0.05	1.41 ± 0.05
28	0.99 ± 0.02	1.64 ± 0.02
34	1.09 ± 0.03	1.80 ± 0.03

Table S2: *Comparison between the calculated activation volume values in cm^3/mol and Å^3/atom for all the different disorders, by using the extended Eq. 3, where compressibility β Gruneisen parameter γ are included.*

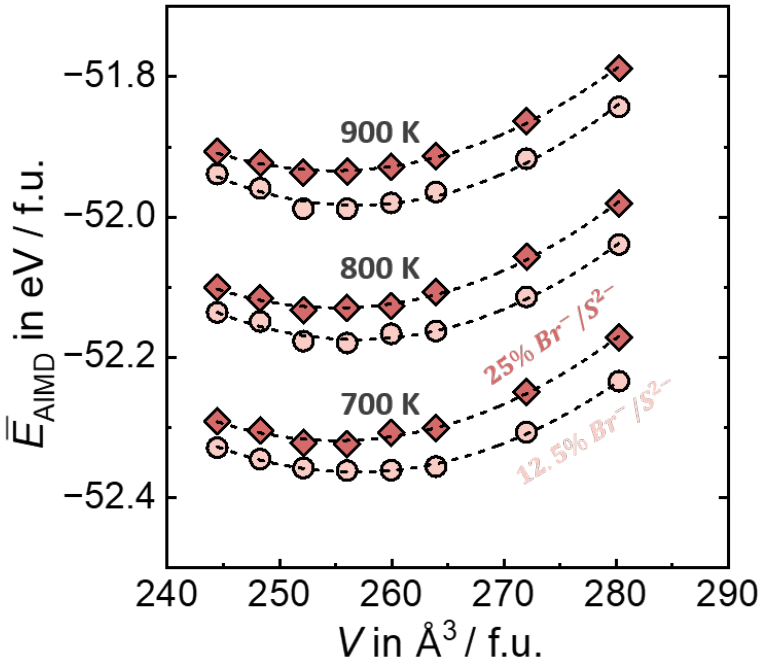

Figure S15: *Averaged energy from AIMD simulations at volumes and the fitted Birch-Murnaghan EOS. The circle points depict the 12.5% site disorder, while the rhombohedral points show the 25% site disorder. Both x and y axis are normalized to one formula unit.*

The Gruneisen parameter, γ, was calculated using the following equations:[4]

Where, the bulk modulus, B = 29 GPa and Shear modulus G = 9.3 GPa extracted from the reported values in the literature.[5]

$$\gamma \approx \frac{3}{2} \cdot \frac{(3-4x^2)}{(1+2x^2)} \tag{S14}$$

$$x = \frac{V_T}{V_L} = \sqrt{\frac{G_{VRH}}{B_{VRH}+(4/3)G_{VRH}}} \tag{S15}$$

In order to find out if there are any changes in the site disorder after the applied pressure, we present the X-ray diffraction patterns for the various Br^-/S^{2-} site disorder. Rietveld refinements reveal that the site disorder does not change in the materials after the applied pressure, within the uncertainty. The exact value of the site disorders with the uncertainties can be found in the following Table S3.

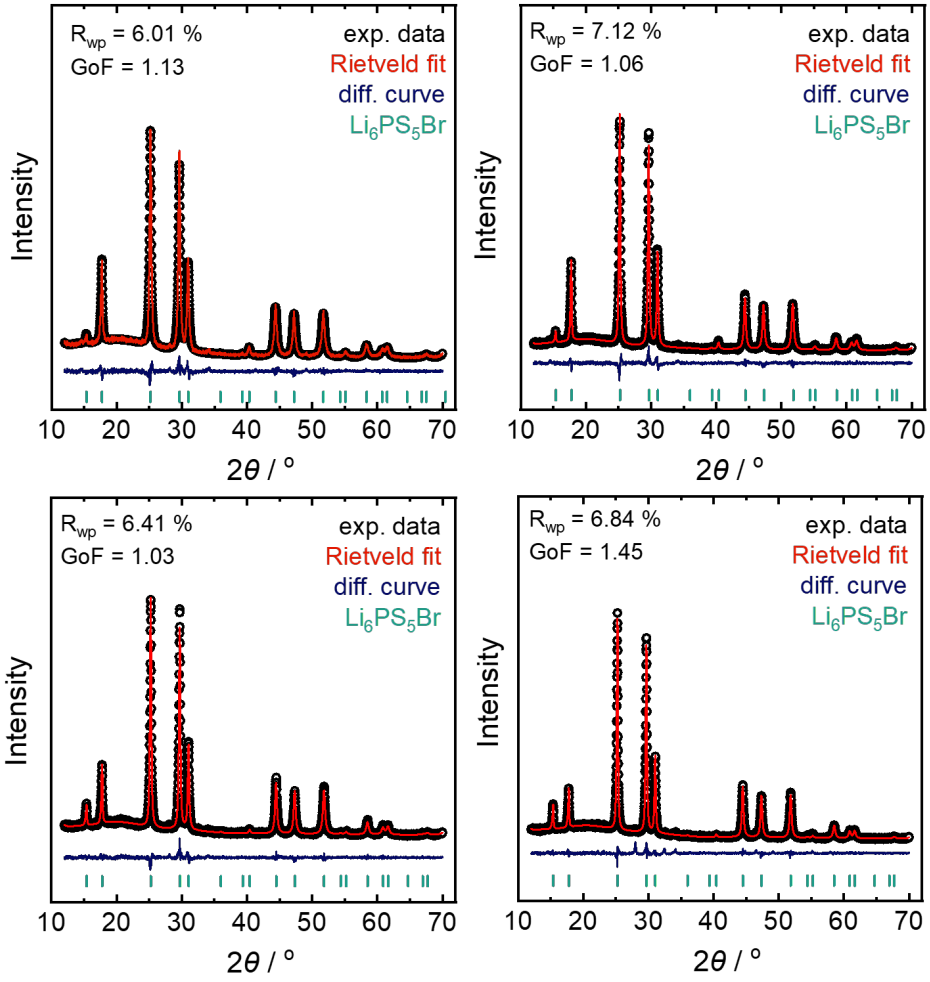

Figure S16: *X-ray diffraction data and the corresponding Rietveld refinements of the various Br^-/S^{2-} site-disordered Li_6PS_5Br. The black circles represent the experimental data and the red line shows the calculated pattern. The blue line denotes the difference profile. The green vertical lines denote the Bragg reflection position from Li_6PS_5Br.*

Br^-/S^{2-} site disorder / %	
Before applied pressure	After applied pressure up to 1.5 GPa
10 ± 2	10 ± 3
18 ± 2	18 ± 2
28 ± 3	28 ± 4
34 ± 3	34 ± 4

Table S3: *The Br^-/S^{2-} site disorder does not change with pressure within the uncertainty.*

References

(1) Mehrer, H. *Diffusion in Solids*; Springer Series in Solid-State Sciences; Springer Berlin Heidelberg: Berlin, Heidelberg, 2007; Vol. 155. https://doi.org/10.1007/978-3-540-71488-0.

(2) Mellander, B.-E.; Lazarus, D. Electrical Conductivity and Activation Volume for α - Li 2 SO 4. *Phys. Rev. B* **1985**, *31* (10), 6801–6803. https://doi.org/10.1103/PhysRevB.31.6801.

(3) Yoon, D. N.; Lazarus, D. Pressure Dependence of Ionic Conductivity in KCl, NaCl, KBr, and NaBr. *Phys. Rev. B* **1972**, *5* (12), 4935–4945. https://doi.org/10.1103/PhysRevB.5.4935.

(4) Agne, M. T.; Anand, S.; Snyder, G. J. Inherent Anharmonicity of Harmonic Solids. *Research* **2022**, *2022*. https://doi.org/10.34133/2022/9786705.

(5) Deng, Z.; Wang, Z.; Chu, I.-H.; Luo, J.; Ong, S. P. Elastic Properties of Alkali Superionic Conductor Electrolytes from First Principles Calculations. *J. Electrochem. Soc.* **2016**, *163* (2), A67–A74. https://doi.org/10.1149/2.0061602jes.